Thermodynamics of ^{3}He in ^{3}He-^{4}He thin films: The Fermi gas limit

R. H. Anderson and M. D. Miller*
Department of Physics, Washington State University, Pullman, Washington 99164-2814
(Received 15 July 2002; published 13 November 2002)

We examine the thermodynamics of a two-dimensional Fermi gas model describing adsorbed ^{3}He in a thin superfluid ^{4}He film. The ^{3}He system is characterized by both a hydrodynamic effective mass and a set of discrete transverse single-particle states that model the effects of the interaction with the substrate that supports the film. We show that the magnetization steps seen in experiment are a simple manifestation of the $T=0$ K equation of state. We prove that perfectly horizontal magnetization steps rigorously disappear at any finite temperature. We show that the thermal stability of the steps is determined by the larger of $\Delta\epsilon/2$, one-half of the level spacing, and $\mu_m\mathcal{H}_0$, the magnetic energy. We derive the conditions under which there exist points in the phase space (termed invariant points) through which all low-temperature isotherms pass exponentially close. The invariant points appear for magnetization versus ^{3}He coverage, chemical potential versus magnetization, magnetic susceptibility versus coverage, and speed of sound squared versus coverage. We compare our calculated invariant points for the magnetization versus coverage with experiment and find good agreement. We show that there exist small regions of thermodynamic phase space in which the temperature derivative of the pressure is negative. We explain these anomalous regions as the result of ^{3}He atoms ''spilling over'' from a full Fermi sea to an empty Fermi sea upon the application of a small increase in temperature. Through a Maxwell relation, this behavior can also be seen as in the appearance of a local peak in low-temperature entropy isotherms versus coverage. In the limit of a two state model, we calculate the specific heat and show that a Schottky peak develops in the low ^{3}He coverage limit. We calculate the magnetic susceptibility and predict that it should exhibit a steplike structure versus ^{3}He coverage similar to that of the magnetization. We calculate the speed of sound and show that it should exhibit zero-temperature discontinuities at the points where new Fermi seas begin to be occupied. Both the steplike structure in the magnetic susceptibility and the discontinuity-type structure in the speed of sound persist to temperatures on the order of 100 mK, and are analyzed in terms of invariant points in their respective phase diagrams. We show explicitly that, in the Fermi gas limit, the zero-field magnetic susceptibility is simply proportional to the isothermal compressibility.

DOI: 10.1103/PhysRevB.66.174511 PACS number(s): 67.70.+n, 67.60.Fp, 64.30.+t

I. INTRODUCTION

In 1989, an important advance in the understanding of the properties of thin ^{3}He-^{4}He mixture films was made by Higley, Sprague, and Hallock by their discovery of steps in the magnetic equation of state (magnetization isotherms versus coverage).[1,2] In these systems, the ^{3}He atoms reside near the upper surface of the superfluid ^{4}He film and are localized in the direction transverse to the film by the external potentials due to the ^{4}He film and the solid substrate that supports the combined helium systems. As pointed out by Hallock and Higley *et al.*,[2] the steps are direct evidence of the existence of this set of discrete ^{3}He states and, further, the experimental data can be analyzed to yield properties of the states. These states were first predicted and examined by Gasparini and co-workers in a pioneering series of heat capacity experiments on the mixture films.[3–5] In both the Hallock and Gasparini experiments, the solid substrate was Nuclepore, a polycarbonate material threaded by roughly cylindrical passages of nominal diameter 2000 Å.

The ^{3}He subsystem forms a quasi two-dimensional Fermi system whose properties have been examined by a number of authors.[6–9] In Ref. 2, Higley, Sprague, and Hallock showed that a Fermi gas model with the effects of interaction included through the use of phenomenological Fermi liquid parameters enable them to obtain excellent fits to their data. In this paper, we take a step back, in a sense, and ask what behavior is to be expected in the absence of interactions, in the limit that the ^{3}He atoms are treated as ideal fermion quasiparticles. In that limit, much of the analysis can be performed analytically and we will show that this model is capable of qualitatively explaining the behavior of the true mixture film. In Sec. II, we will derive the ground-state properties and show why a stepped structure in the magnetization versus areal density is to be expected. We will also examine in detail the behavior of the chemical potential and spreading pressure. In particular, we point out that the ground-state pressure and chemical potential are continuous but not differentiable at those densities corresponding to the beginning and end of the steps and the speed of sound is discontinuous at those points. In Sec. III, we shall derive the relevant statistical mechanics of this two-dimensional ideal Fermi gas model. In Sec. IV, we discuss the finite temperature behavior in terms of the numerical solution of a two-state model. The parameters for the model are determined by experiment. We examine isotherms of the magnetization versus ^{3}He coverage, and show that there exist points in the phase diagram through which all low-temperature isotherms pass exponentially close. We denote such points as *invariant points*. These invariant points are also found in the phase diagrams of chemical potential versus magnetization, magnetic susceptibility versus coverage and speed of sound (squared) versus coverage. The existence of these invariant points determines qualitatively the energy scale over which the phase diagram

TABLE I. The values of various parameters used for the numerical calculations.

Quantity	Symbol	Value
Single particle ground state	ϵ_0^0	0.0 K
Single particle first excited state	ϵ_1^0	1.8 K
^{3}He effective mass	m^*	$1.38m_3$
^{3}He magnetic moment	μ_m	7.7824×10^{-4} K/T
Applied magnetic field	$\mathcal{H}_0$	2 T
Density of ^{3}He at monolayer completion	$n_{\diagup}$	0.0647 Å^{-2}
Fermi energy of ^{3}He at monolayer completion	$\epsilon_{\mathrm{F}\diagup}$	2.37 K
Onset coverage for first excited state occupation	$\overline{n}_{\mathrm{onset}}$	0.761

retains its global structure. This analysis explains why the relevant energy scale for the magnetization steps is the level spacing (1.8 K) and not the magnetic energy (30 mK). We show that the zero-temperature kinklike structure for the ground-state pressure versus density has the interesting consequence at finite temperature of leading to regions in which the pressure has a negative temperature derivative. This result is also explained in terms of a physical model based on the ''spilling over'' of ^{3}He atoms from a filled Fermi sea to an empty Fermi sea upon the application of a small increase in temperature. In Sec. IV, we obtain analytic expressions for the heat capacity at constant area and constant pressure, the magnetic susceptibility, the isothermal compressibility, and the thermal expansion coefficient. Further, we show that the magnetic susceptibility versus coverage will exhibit a steplike structure similar to the magnetization and also that the speed of sound (squared) will show a discontinuity–type structure as a function of coverage. Both phase diagrams are analyzed in terms of their invariant points. Section V is the conclusion.

II. GROUND STATE

We consider a system of $\mathcal{N}$ ^{3}He atoms in an area $\mathcal{A}$. The spin-$\frac{1}{2}$ atoms have a magnetic moment μ_m and are subject to an applied magnetic field $\mathcal{H}_0$. The spin state will be labeled by the index $s=\pm$ where we can arbitrarily choose $s=+$ to represent the low energy configuration. The ^{3}He atoms are adsorbed onto a film of ^{4}He which is itself adsorbed onto a solid substrate. All information in the ^{3}He system concerning the ^{4}He film and the substrate is contained in a set of transverse single-particle states whose energy levels are denoted $\{\epsilon_\alpha^0\}$. Thus the energy of a ^{3}He quasiparticle in state $\{\alpha,s,\mathbf{k}\}$, where $\mathbf{k}$ is the two-dimensional wave vector, is given by

$$\epsilon_{\mathbf{k}}^{\alpha,s}=\epsilon_\alpha^0+\frac{\hbar^2k^2}{2m^*}-\mu_m\mathcal{H}_0 s. \tag{2.1}$$

$m^*=1.38m_3$ is the hydrodynamic effective mass determined by Higley, Sprague, and Hallock,[2] and $\mu_M=7.7824\times10^{-4}$ K/T. It is at this stage that interactions between the quasiparticles are neglected. We note that DiPirro and Gasparini were the first to describe the adsorbed ^{3}He system as an ideal Fermi gas with a discrete set of transverse single-particle states.[3] In the numerical work to be described below, we shall use $\mathcal{H}_0=2$ T to agree with the NMR experiments of Ref. 2. The values of the parameters in Eq. (2.1) are collected together in Table I.

We begin the ground-state analysis by imagining a ^{4}He film with one ^{3}He atom present. We turn on the external field $\mathcal{H}_0$, then each ^{3}He single particle level ϵ_α^0 is split by an amount $2\mu_m\mathcal{H}_0$. We begin adding ^{3}He atoms to the system. The interaction in Eq. (2.1) is attractive for parallel spins and the first ^{3}He atoms begin filling the Fermi sea $\{\alpha=0,s=+\}$. Each atom contributes a magnetic moment μ_m and so, after $\mathcal{N}$ atoms have been added, the magnetization in this regime is simply $\mathcal{N}\mu_m$. That is, the magnetization increases linearly with the number of ^{3}He atoms that are added. This is the first ramp and is illustrated in Fig. 1.

At the density n_{0L} the bottom of the ϵ_{0-} band is reached. Further addition of ^{3}He atoms fills both bands jointly, and so contributes zero net magnetization. This creates the first step

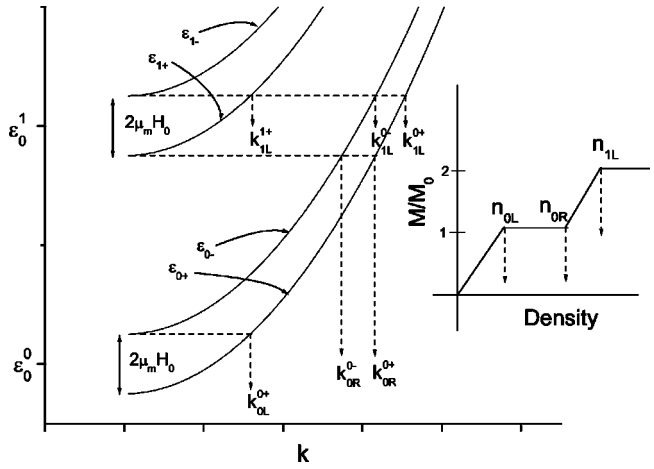

FIG. 1. The main plot shows single particle energies as a function of wave vector k. The bands forming out of the two transverse states, ϵ_0^0 and ϵ_1^0, are split by $2\mu_m\mathcal{H}_0$. For $k<k_{0L}^{0+}$ only the lowest state ϵ_{0+} is occupied. In this regime, the magnetization grows linearly with the number of ^{3}He atoms as shown in the inset. Adding more ^{3}He fills the two states ϵ_{0+} and ϵ_{0-} jointly, and thus there is no change in the overall magnetization. These branches reach the bottom of the ϵ_{1+} band at the wave vectors denoted by k_{0R}^{0-} and k_{0R}^{0+}. This region of unchanging magnetization thus forms the first step as indicated in the inset for densities between n_{0L} and n_{0R}. Additional ramps and steps are formed in the same manner.

as shown in the inset of Fig. 1. When the density reaches n_{0R}, the bottom of the ϵ_{1+} band is reached and so a linear magnetization regime is produced. This is the second ramp shown in the inset of Fig. 1. In this manner, the magnetization versus density relation is created in a stepped structure at zero temperature. In the following, we shall derive the quantitative properties of these magnetization steps.

The number of atoms in occupied level $\{\alpha,s\}$ is given by

$$\mathcal{N}_{\alpha s}=\frac{k_{\mathrm{F}\alpha s}^2}{4\pi}\mathcal{A}. \tag{2.2}$$

Thus the Fermi wave vector for each level is given by

$$k_{\mathrm{F}\alpha s}^2=4\pi n_{\alpha s}, \tag{2.3}$$

where $n_{\alpha s}=\mathcal{N}_{\alpha s}/\mathcal{A}$. The total density is given by

$$\overline{n}=\sum_{\alpha,s}\frac{n_{\alpha s}}{n_{\diagup}}, \tag{2.4}$$

where the dimensionless density, called the *coverage* $\overline{n}$, is measured in units of one complete ^{3}He monolayer $n_{\diagup}=0.0647$ Å^{-2} (see Ref. 2 and Table I).

The internal energy $\mathcal{U}$ is given by

$$\mathcal{U}=\sum_{\alpha,s}\left[\epsilon_\alpha^0-\mu_m\mathcal{H}_0 s+\frac{1}{2}\epsilon_{\mathrm{F}\alpha s}\right]\mathcal{N}_{\alpha s}, \tag{2.5}$$

where $\epsilon_{\mathrm{F}\alpha s}$ is the *partial* Fermi energy (i.e., $\frac{1}{2}\epsilon_{\mathrm{F}\alpha s}$ is the kinetic energy contribution) for the level $\{\alpha,s\}$, and is defined by

$$\epsilon_{\mathrm{F}\alpha s}=\frac{\hbar^2k_{\mathrm{F}\alpha s}^2}{2m^*}=\frac{\hbar^2}{2m^*}(4\pi n_{\alpha s}). \tag{2.6}$$

The chemical potential μ for *occupied* level $\{\alpha,s\}$ is given by

$$\mu=\left(\frac{\partial\mathcal{U}}{\partial\mathcal{N}_{\alpha s}}\right)_{\mathcal{A}}=\epsilon_\alpha^0-\mu_m\mathcal{H}_0 s+\epsilon_{\mathrm{F}\alpha s}, \tag{2.7}$$

and the spreading pressure $\mathcal{P}$ is therefore

$$\mathcal{P}=-\left(\frac{\partial\mathcal{U}}{\partial\mathcal{A}}\right)_{\mathcal{N}}=\frac{1}{2}\sum_{\alpha,s}\epsilon_{\mathrm{F}\alpha s}n_{\alpha s}. \tag{2.8}$$

By inspection of Eqs. (2.5) and (2.8) we find

$$\mathcal{U}=\sum_{\alpha,s}[\epsilon_\alpha^0-\mu_m\mathcal{H}_0 s]\mathcal{N}_{\alpha s}+\mathcal{P}\mathcal{A}. \tag{2.9}$$

Using Eq. (2.9), the enthalpy, $\mathcal{H}=\mathcal{U}+\mathcal{P}\mathcal{A}$, can be written as

$$\mathcal{H}=\sum_{\alpha,s}[\epsilon_\alpha^0-\mu_m\mathcal{H}_0 s]\mathcal{N}_{\alpha s}+2\mathcal{P}\mathcal{A}. \tag{2.10}$$

Both Eqs. (2.9) and (2.10) are also valid at finite temperature if $\mathcal{N}_{\alpha s}$ is interpreted as an average occupation number; see Eq. (3.1) below. In the ground state, we can use Eq. (2.8) to simplify Eq. (2.10)

$$\mathcal{H}=\sum_{\alpha,s}[\epsilon_\alpha^0-\mu_m\mathcal{H}_0 s+\epsilon_{\mathrm{F}\alpha s}]\mathcal{N}_{\alpha s}. \tag{2.11}$$

Finally, from Eq. (2.7), we find that Eq. (2.11) reduces to $\mathcal{H}=\mu\mathcal{N}$, the expected result at absolute zero.

Referring to the inset of Fig. 1, we define the densities at the beginning (left hand side) and the end (right hand side) of the first step as n_{0L} and n_{0R}, respectively. The densities are determined by equating the chemical potentials for the occupied bands at those points. Thus, at $n=n_{0L}$, we have $\mu(0,+,n_{0L})=\mu(0,-,n_{0L})$, which yields

$$n_{0L}=\frac{m^*\mu_m\mathcal{H}_0}{\pi\hbar^2}. \tag{2.12}$$

In terms of the coverage we can write

$$\overline{n}_{0L}=\frac{\mu_m\mathcal{H}_0}{\epsilon_{\mathrm{F}\diagup}}, \tag{2.13}$$

and $\epsilon_{\mathrm{F}\diagup}=2.37$ K is the Fermi energy of a completed monolayer:

$$\epsilon_{\mathrm{F}\diagup}=\frac{\hbar^2}{2m^*}(2\pi n_{\diagup}). \tag{2.14}$$

At the density n_{0R}, we set $\mu(0,+,n_{0R})=\mu(0,-,n_{0R})=\mu(1,+,n_{0R})$ to find

$$\overline{n}_{0R}+\overline{n}_{0L}=\overline{n}_{\mathrm{onset}}, \tag{2.15}$$

where, $\overline{n}_{0L}$ is defined in Eq. (2.13) and

$$\overline{n}_{\mathrm{onset}}=\frac{\Delta\epsilon_0}{\epsilon_{\mathrm{F}\diagup}}. \tag{2.16}$$

The quantity $\Delta\epsilon_0=\epsilon_1^0-\epsilon_0^0$ is the level spacing and $\overline{n}_{\mathrm{onset}}$ is the onset coverage. This is the coverage at which the first excited state would begin to be occupied in the *absence* of an external field. For a given external field, the width of the step, $\overline{n}_{0R}-\overline{n}_{0L}$, is proportional to the level spacing.

The total magnetization is defined by

$$\mathcal{M}=\mu_m\sum_\alpha(\mathcal{N}_{\alpha,+}-\mathcal{N}_{\alpha,-}). \tag{2.17}$$

Using Eq. (2.12), the value of the magnetization at the first step is given by

$$\mathcal{M}_0=\frac{m^*\mu_m^2\mathcal{H}_0\mathcal{A}}{\pi\hbar^2}. \tag{2.18}$$

This result can be generalized to any step. If we temporarily introduce a state dependent effective mass, m_α^*, then the *increase* in magnetization at the end of the αth ramp is given by

$$\Delta\mathcal{M}_\alpha=\frac{m_\alpha^*\mu_m^2\mathcal{H}_0\mathcal{A}}{\pi\hbar^2}. \tag{2.19}$$

TABLE II. Pressure and partial densities for the first two ramps and steps in the ground-state magnetization equation of state.

Density range	Partial densities	Pressure
$0 \leqslant n \leqslant n_{0L}$	$n_{0+}=n$	$\mathcal{P}=\hbar^2 2\pi(n^2)/2m^*$
$n_{0L} \leqslant n \leqslant n_{0R}$	$n_{0+}=\frac{1}{2}(n+n_{0L})$	$\mathcal{P}=\hbar^2 2\pi(\frac{1}{2}n^2+\frac{1}{2}n_{0L}^2)/2m^*$
	$n_{0-}=\frac{1}{2}(n-n_{0L})$	
$n_{0R} \leqslant n \leqslant n_{1L}$	$n_{0+}=\frac{1}{3}(n+n_{0L}+\frac{1}{2}n_{\rm onset})$	$\mathcal{P}=\hbar^2 2\pi(\frac{1}{3}n^2+\frac{1}{3}(2n_{0L}^2-n_{0L}n_{\rm onset}+\frac{1}{2}n_{\rm onset}{}^2))/2m^*$
	$n_{0-}=\frac{1}{3}(n-2n_{0L}+\frac{1}{2}n_{\rm onset})$	
	$n_{1+}=\frac{1}{3}(n-n_{0R})$	
$n_{1L} \leqslant n \leqslant n_{1R}$	$n_{0+}=\frac{1}{4}(n+2n_{0L}+n_{\rm onset})$	$\mathcal{P}=\hbar^2 2\pi(\frac{1}{4}n^2+n_{0L}^2+\frac{1}{4}n_{\rm onset}{}^2)/2m^*$
	$n_{0-}=\frac{1}{4}(n-2n_{0L}+n_{\rm onset})$	
	$n_{1+}=\frac{1}{4}(n+2n_{0L}-n_{\rm onset})$	
	$n_{1-}=\frac{1}{4}(n-n_{1L})$	

Thus the ratio of the increase in magnetization at the αth step relative to the magnetization of the first step, $\alpha=0$, is simply the ratio of the effective masses:

$$\Delta\mathcal{M}_\alpha/\mathcal{M}_0=m_\alpha^*/m_0^*. \tag{2.20}$$

The experiment of Ref. 2 provides a data point that is not inconsistent with equal magnetization jumps at the first and second steps. (We note that the authors of Ref. 2 defined $\mathcal{M}_0$ using the *bare* ^{3}He mass, and therefore their magnetizations did not fall on steps with integer values.) As indicated in Table I, in this paper we shall use a single state independent effective mass set equal to the hydrodynamic mass as determined in Ref. 2. We introduce a dimensionless magnetization $\overline{m}$, defined by

$$\overline{m}=\frac{\mathcal{M}}{\mathcal{M}_0}, \tag{2.21}$$

that is essentially the magnetization per unit area.

With a state independent effective mass, we can straightforwardly generalize the above analysis of the first magnetization step to an arbitrary step. We examine the αth step (that is, the step where the states $\{\alpha,\pm\}$ are being jointly filled). In order to determine the density at the left hand edge, $n_{\alpha L}$, we need to equate the $2\alpha+2$ chemical potentials $\mu(\{\nu=0,1,\ldots,\alpha\},\pm,n_{0L})$. This set of equations yields

$$\overline{n}_{\alpha L}=\frac{1}{\epsilon_{\rm F}\not{\prime}}\sum_{\nu=0}^{\alpha-1}(\epsilon_\alpha^0-\epsilon_\nu^0)+(\alpha+1)\overline{n}_{0L}. \tag{2.22}$$

Similarly, for the density at the right hand edge, $n_{\alpha R}$, we need to equate the $2\alpha+3$ chemical potentials $\mu(\{\nu=0,1,\ldots,\alpha\},\pm,n_{0R}),\mu(\alpha+1,-,n_{0R})$. This set of equations yields

$$\overline{n}_{\alpha R}=\frac{1}{\epsilon_{\rm F}\not{\prime}}\sum_{\nu=0}^{\alpha}(\epsilon_{\alpha+1}^0-\epsilon_\nu^0)-(\alpha+1)\overline{n}_{0L}. \tag{2.23}$$

Adding Eqs. (2.23) and (2.22), we find

$$\overline{n}_{\alpha R}+\overline{n}_{\alpha L}=\frac{1}{\epsilon_{\rm F}\not{\prime}}\sum_{\nu=0}^{\alpha-1}(\epsilon_{\alpha+1}^0+\epsilon_\alpha^0-2\epsilon_\nu^0)+\frac{\Delta\epsilon_\alpha}{\epsilon_{\rm F}\not{\prime}}, \tag{2.24}$$

where $\Delta\epsilon_\alpha=\epsilon_{\alpha+1}^0-\epsilon_\alpha^0$. Equation (2.24) is the desired generalization of Eq. (2.15) to steps with $\alpha>0$.

The total magnetization at a density corresponding to the filling of the αth ramp (that is, the unpaired state is $\{\alpha,+\}$) is given by

$$\overline{m}(\alpha)=\frac{\overline{n}-\overline{n}_{\alpha-1R}}{(2\alpha+1)\overline{n}_{0L}}+\alpha, \tag{2.25}$$

where it is understood that $\overline{n}_{-1R}=0$, and from Eqs. (2.22) and (2.23), we have used

$$\overline{n}_{\alpha+1L}-\overline{n}_{\alpha R}=(2\alpha+3)\overline{n}_{0L}. \tag{2.26}$$

The density width of the αth ramp *increases* linearly with α.

In Table II, we display the partial densities and pressures for the first and second ramps and steps as sketched in Fig. 1. We note that the coefficient of the density for the pressure in each region has a term like 1/(number of occupied Fermi seas). The pressure is a series of parabolas that are joined at the corners of the steps. The parabolas on the high density (right hand) side have a smaller curvature than the parabola on the lower density (left hand) side. Thus, the pressure versus density is continuous but not differentiable at the densities corresponding to the corners of the steps $\{\overline{n}_{\alpha L},\overline{n}_{\alpha R},\alpha=0,1,\ldots\}$. From Eq. (2.9), the internal energy on the ramps and steps follows immediately from the entries in Table II.

The dependence of the chemical potential on the magnetization will be a useful quantity for the analysis of the magnetization equation of state. In Table III we write down expressions for the chemical potential along the first two ramps and steps. One can generalize these results to any ramp and step. Thus, the chemical potential along the αth step is given by

TABLE III. Chemical potentials and magnetizations for the first two ramps and steps in the ground-state magnetization equation of state from Eqs. (2.25), (2.27), and (2.28).

Density range	Magnetization	Chemical potential
$0 \leqslant n \leqslant n_{0L}$	$\bar{m} = \bar{n}/\bar{n}_{0L}$	$\mu = \epsilon_0^0 + 2\mu_m \mathcal{H}_0(\bar{m} - 1/2)$
$n_{0L} \leqslant n \leqslant n_{0R}$	$\bar{m} = 1$	$\mu = \epsilon_0^0 + \mu_m \mathcal{H}_0(\bar{n}/\bar{n}_{0L})$
$n_{0R} \leqslant n \leqslant n_{1L}$	$\bar{m} = 1 + (\bar{n} - \bar{n}_{0R})/3\bar{n}_{0L})$	$\mu = \epsilon_1^0 + 2\mu_m \mathcal{H}_0(\bar{m} - 3/2)$
$n_{1L} \leqslant n \leqslant n_{1R}$	$\bar{m} = 2$	$\mu = \frac{1}{2}(\epsilon_0^0 + \epsilon_1^0) + \frac{1}{2}\mu_m \mathcal{H}_0(\bar{n}/\bar{n}_{0L})$

$$\mu = \left(\frac{1}{1+\alpha}\right)\left[\sum_{\nu=0}^{\alpha} \epsilon_\nu^0 + \mu_m \mathcal{H}_0(\bar{n}/\bar{n}_{0L})\right]. \tag{2.27}$$

Similarly, the chemical potential along the αth ramp is given by

$$\mu = \epsilon_\alpha^0 + 2\mu_m \mathcal{H}_0\left(\bar{m} - \alpha - \frac{1}{2}\right) \tag{2.28}$$

where $\alpha = 0,1, \ldots$.

III. FINITE TEMPERATURE

The average number of particles in level $\{\alpha,s\}$ at temperature $\mathcal{T}$, $\beta = 1/k_B\mathcal{T}$, is given by

$$\mathcal{N}_{\alpha,s} = \sum_{\mathbf{k}} \frac{1}{\Lambda_{\alpha,s}^{-1}\exp(\beta\epsilon_{\mathbf{k}}) + 1}, \tag{3.1}$$

where we have introduced

$$\epsilon_{\mathbf{k}} = \hbar^2 k^2/2m^*, \tag{3.2}$$

$$\Lambda_{\alpha,s} = e^{\beta(\mu - \epsilon_\alpha^0 + \mu_m \mathcal{H}_0 s)}. \tag{3.3}$$

In two dimensions, the integral in Eq. (3.1) can be done analytically. It will prove to be useful to mimic the three-dimensional analysis of the ideal Fermi gas by writing

$$\mathcal{N}_{\alpha,s} = \mathcal{A}\frac{1}{\lambda_T^2} G_1(\Lambda_{\alpha,s}), \tag{3.4}$$

where $\lambda_T^2 = (2\pi\hbar^2)/(m^* k_B T)$ is the thermal de Broglie wavelength squared, and we have defined a general power series in $\Lambda_{\alpha,s}$ as

$$G_\nu(\Lambda_{\alpha,s}) = -\sum_{l=1}^{\infty} \frac{(-\Lambda_{\alpha,s})^l}{l^\nu}, \quad \nu = 1,2, \ldots. \tag{3.5}$$

Using $G_1(\Lambda_{\alpha,s}) = \ln(1+\Lambda_{\alpha,s})$, the partial density can be written

$$n_{\alpha s} = \frac{1}{\lambda_T^2}\ln(1+\Lambda_{\alpha,s}). \tag{3.6}$$

We note that this result can be obtained directly from Eq. (3.1) and is therefore valid at all temperatures.

We can now write down the dimensionless densities and magnetization introduced in Sec. II,

$$\bar{n} = \sum_{\alpha,s} \bar{n}_{\alpha,s}, \tag{3.7}$$

$$\bar{n}_{\alpha,s} = \frac{1}{2w_{/\!/}}\ln(1+\Lambda_{\alpha,s}), \tag{3.8}$$

where $w_{/\!/} = \beta\epsilon_{\mathrm{F}/\!/}$, and

$$\bar{m} = \sum_{\alpha} \bar{m}_\alpha, \tag{3.9}$$

$$\bar{m}_\alpha = \frac{1}{2x}\ln\left(\frac{1+\Lambda_{\alpha+}}{1+\Lambda_{\alpha-}}\right), \tag{3.10}$$

where $x = \beta\mu_m\mathcal{H}_0$. A summary of the notation used for the finite temperature problem can be found in Table IV.

Inverting Eq. (3.6) yields

$$\Lambda_{\alpha,s} = e^{\beta\epsilon_{\mathrm{F}\alpha s}} - 1, \tag{3.11}$$

where $\epsilon_{\mathrm{F}\alpha s} = (\hbar^2/2m^*)4\pi n_{\alpha s}(\mathcal{T})$ is the *finite-temperature generalization* of the quantity that was introduced in Eq. (2.6). Alternatively, we have the identity

$$\beta\epsilon_{\mathrm{F}\alpha s} = n_{\alpha s}\lambda_T^2. \tag{3.12}$$

From Eq. (3.11), the chemical potential can be written

$$\mu = \epsilon_\alpha^0 - \mu_m\mathcal{H}_0 s + \frac{1}{\beta}\ln(e^{\beta\epsilon_{\mathrm{F}\alpha s}} - 1). \tag{3.13}$$

For additional discussion concerning the properties of the chemical potential in a two-dimensional polarized fermion

TABLE IV. Summary of the notation used for the finite-temperature system. From Table I, the values of the quantities used for the numerical work are $\mu_m\mathcal{H}_0 = 15.6$ mK, $\Delta\epsilon = 1.8$ K, and $\epsilon_{\mathrm{F}/\!/} = 2.37$ K.

Symbol	Meaning
$y_{\alpha,s}$	$\beta(\mu - \epsilon_\alpha^0 + \mu_m\mathcal{H}_0 s)$
$\Lambda_{\alpha,s}$	$\exp(y_{\alpha,s})$
x	$\beta\mu_m\mathcal{H}_0$
w	$\beta\Delta\epsilon$
$w_{/\!/}$	$\beta\epsilon_{\mathrm{F}/\!/}$
$\epsilon_{\mathrm{F}\alpha s}$	$(\hbar^2/2m^*)4\pi n_{\alpha s}(\mathcal{T})$
$\epsilon_{\mathrm{F}0}$	$(\hbar^2/2m^*)2\pi n$

system, see Ref. 10. In the low-temperature regime, $\beta\epsilon_{\mathrm{F}\alpha s}>1$, it is convenient to rewrite Eq. (3.13) as

$$\mu=\epsilon_\alpha^0-\mu_m\mathcal{H}_0 s+\epsilon_{\mathrm{F}\alpha s}-\frac{1}{\beta}\sum_{l=1}^{\infty}\frac{e^{-l\beta\epsilon_{\mathrm{F}\alpha s}}}{l}. \tag{3.14}$$

In the degenerate limit, with $\mathcal{N}$ and $\mathcal{A}$ fixed, Eq. (3.14) can be used to show that finite-temperature corrections for the chemical potential are of exponential order. Here and henceforth, we shall use the term *exponential order* to denote a quantity that vanishes in the $\lim\mathcal{T}\to 0$ in the nonanalytic form $\exp(-\text{constant}/\mathcal{T})$.

The pressure can be written

$$\mathcal{P}=\frac{1}{\beta\mathcal{A}}\sum_{\alpha,s,\mathbf{k}}\ln(1+\Lambda_{\alpha,s}e^{-\beta\epsilon_{\mathbf{k}}}), \tag{3.15}$$

that can alternatively be put in the form

$$\mathcal{P}=\frac{1}{\beta\lambda_T^2}\sum_{\alpha,s}G_2(\Lambda_{\alpha,s}), \tag{3.16}$$

where the sum G_2 is defined in Eq. (3.5). Unfortunately, G_2 has no simple analytic form. Further, this series converges only in the classical regime ($\Lambda_{\alpha,s}<1$). One can, however, derive an alternative exact expression that is useful in the quantum regime. Following the low-temperature analysis introduced in Ref. 11 one begins with Eq. (3.15) in the form

$$\mathcal{P}=\frac{1}{\beta\lambda_T^2}\sum_{\alpha,s}\int_0^\infty dx\frac{x}{e^{x-y_{\alpha,s}}+1}, \tag{3.17}$$

where for convenience we have introduced the notation $\Lambda_{\alpha,s}=e^{y_{\alpha,s}}$. We now change variables to $z=x-y_{\alpha,s}$ and separate the expression into two terms

$$\mathcal{P}=\frac{1}{\beta\lambda_T^2}\sum_{\alpha,s}\left(\int_0^{y_{\alpha,s}}dz\frac{(-z+y_{\alpha,s})}{e^{-z}+1}+\int_0^\infty dz\frac{(z+y_{\alpha,s})}{e^z+1}\right). \tag{3.18}$$

The first integral can be reduced using the identity

$$\frac{1}{e^{-z}+1}=1-\frac{1}{e^z+1}. \tag{3.19}$$

We then immediately find

$$\mathcal{P}=\frac{1}{\beta\lambda_T^2}\sum_{\alpha,s}\left(\frac{1}{2}y_{\alpha,s}^2+\frac{\pi^2}{6}+\sum_{l=1}^{\infty}(-)^l\frac{e^{-ly_{\alpha,s}}}{l^2}\right). \tag{3.20}$$

This expression for the pressure is exact and the inner summation converges absolutely for $y_{\alpha,s}=\beta(\mu-\epsilon_\alpha^0+\mu_m\mathcal{H}_0 s)>0$. For $y_{\alpha,s}=0$, that sum equals $-\pi^2/12$. We can also use Eq. (3.5) to write the low-temperature form as

$$\mathcal{P}=\frac{1}{\beta\lambda_T^2}\sum_{\alpha,s}\left[\frac{1}{2}y_{\alpha,s}^2+\frac{\pi^2}{6}-G_2\left(\frac{1}{\Lambda_{\alpha,s}}\right)\right], \tag{3.21}$$

that can be compared directly with the high-temperature form [Eq. (3.16)]. As expected, if we use Eq. (3.21) in $n=(\partial\mathcal{P}/\partial\mu)_{\mathcal{T}}$, we immediately recover $n=\Sigma_{\alpha,s}n_{\alpha s}$ with $n_{\alpha s}$ given by Eq. (3.6).

In the degenerate limit, $y_{\alpha,s}\gg 1$, the pressure becomes

$$\lim_{\mathcal{T}\to 0}\mathcal{P}\sim\sum_{\alpha,s}\left[\frac{1}{2}\epsilon_{\mathrm{F}\alpha s}n_{\alpha s}+\frac{\pi^2}{6}\frac{1}{\beta\lambda_T^2}-\frac{1}{\beta\lambda_T^2}e^{-y_{\alpha,s}}+O(e^{-2y_{\alpha,s}})\right]. \tag{3.22}$$

The leading order correction to the pressure at zero temperature is of order T^2 and the corrections to that term are of exponential order. The coefficient of the T^2 term is a constant, independent of the state $\{\alpha,s\}$. The implication is that the low-temperature pressure should have a stepped structure with an additional contribution of $\pi^2/(6\beta\lambda_T^2)$ each time another state is occupied.

The final fundamental thermodynamic quantity that we shall obtain in this section is the entropy. An expression for the entropy can be most easily derived from the defining expression for the Gibbs free energy ($\mu\mathcal{N}=\mathcal{H}-\mathcal{T}S$):

$$S=\frac{1}{\mathcal{T}}(\mathcal{H}-\mu\mathcal{N}). \tag{3.23}$$

Using Eq. (2.10) for the enthalpy and Eq. (3.13) for the chemical potential, we immediately find

$$S/k_{\mathrm{B}}=-\sum_{\alpha,s}y_{\alpha,s}\mathcal{N}_{\alpha s}+2\beta\mathcal{P}\mathcal{A}. \tag{3.24}$$

We can consider this to be $S(\mu,\mathcal{A},\mathcal{T})$. In the low-temperature limit, $n_{\alpha s}\lambda_T^2\gg 1$, we can use Eq. (3.22) for the pressure to obtain to exponential order,

$$\lim_{\mathcal{T}\to 0}S/\mathcal{N}k_B\sim\nu_{\mathrm{occ}}\frac{\pi^2}{6}\left(\frac{k_B\mathcal{T}}{\epsilon_{\mathrm{F}0}}\right), \tag{3.25}$$

where ν_{occ} is the number of occupied levels at zero temperature, and the Fermi energy $\epsilon_{\mathrm{F}0}$ is defined by

$$\epsilon_{\mathrm{F}0}=(\hbar^2/2m^*)2\pi n. \tag{3.26}$$

In Sec. IV, we shall apply the basic thermodynamic results from this section to calculate the magnetic equation of state, equation of state and chemical potential using a two-state model that mimics the experiment of Higley *et al.*[2] We shall also derive general expressions for the heat capacity, magnetic susceptibility, the isothermal compressibility, and the thermal expansion coefficient, and compute numerical results for the two–state model.

IV. RESULTS

In this section, we examine the equation of state of the ideal Fermi gas model of the adsorbed ^{3}He system. As summarized in Table I, for the numerical model we have two

transverse states with energies $\{\epsilon_0^0=0,\epsilon_1^0=1.8\ K\}$ and an effective mass, $m^*=1.38m_3$, whose values were determined experimentally by Higley, Sprague and Hallock.[2] The magnetic energy, $2\mu_m\mathcal{H}_0$, is approximately 31 mK for a 2-T field. In Fig. 2, we show the magnetic equation of state (isotherms of magnetization versus coverage). The evolution of the step structure out of the zero temperature results is clear. We note that the stepped structure is still clear at $\mathcal{T}=100$ mK despite the fact that that temperature is three times larger than the magnetic energy. The selection of temperatures chosen for the isotherms match those in Ref. 2.

Although the slopes of the low-temperature isotherms in Fig. 2 seem to be flat in the region of the center of the zero temperature step, it is straightforward to show that true horizontal steps only occur at absolute zero. The slope of a magnetization isotherm is given by

$$\frac{d\bar{m}}{d\bar{n}}=\left(\frac{1}{\bar{n}_{0L}}\right)\frac{\sum_\alpha\{[\Lambda_{\alpha,+}/(1+\Lambda_{\alpha,+})]-[\Lambda_{\alpha,-}/(1+\Lambda_{\alpha,-})]\}}{\sum_\alpha\{[\Lambda_{\alpha,+}/(1+\Lambda_{\alpha,+})]+[\Lambda_{\alpha,-}/(1+\Lambda_{\alpha,-})]\}}, \tag{4.1}$$

where the derivative is taken at fixed β and $\mathcal{H}_0$. Thus, the condition $(d\bar{m}/d\bar{n})=0$ requires $\Lambda_{\alpha,+}=\Lambda_{\alpha,-}\ \forall\alpha$. At finite temperature, these can be equal only when $\mathcal{H}_0=0$. In the $\lim\beta\to\infty$, $\Lambda_{\alpha,s}\to\infty$; thus the terms in the numerator cancel out to exponential order and create steps for each state α when both spin states are occupied.

There are two aspects of Fig. 2 that we wish to examine. The first is the question of the stability of the step feature. It is clear that the steps survive fairly intact up to a temperature of at least 100 mK. The second is the nature of the two (finite density) points through which all isotherms seem to pass.

In order to examine the stability of the step, we can use Eq. (4.1) to calculate the slope of the isotherm at $\bar{m}=1.0$. We first rewrite Eq. (3.10) as a quadratic equation in Λ_{0+}:

$$(e^{2x\bar{m}}-1)+(1+e^{-w})(e^{2x(\bar{m}-1)}-1)\Lambda_{0+}+e^{-w}(e^{2x(\bar{m}-2)}-1)\Lambda_{0+}^2=0. \tag{4.2}$$

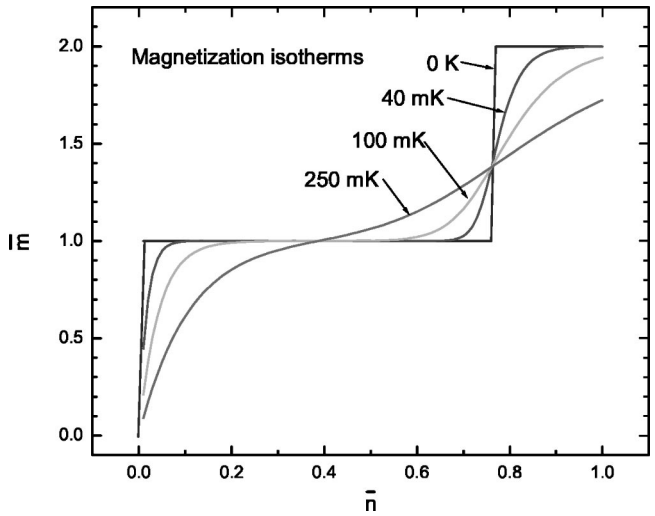

FIG. 2. Magnetization $\bar{m}$ as a function of coverage $\bar{n}$ for temperatures = 0 K, 40 mK, 100 mK, and 250 mK.

For $\bar{m}=1$, Eq. (4.2) can be immediately solved to yield

$$\Lambda_{0,\pm}=e^{\pm x+w/2},\qquad \Lambda_{1,\pm}=e^{\pm x-w/2}. \tag{4.3}$$

Substituting Eqs. (4.3) into Eq. (4.1) yields the slope at $\bar{m}=1$:

$$\left(\frac{d\bar{m}}{d\bar{n}}\right)_{\bar{m}=1}=\left(\frac{1}{\bar{n}_{0L}}\right)\left[\frac{1-e^{-2x}}{1+e^{-x}(e^{w/2}+e^{-w/2})+e^{-2x}}\right]. \tag{4.4}$$

In the low-temperature limit, with $\Delta\epsilon\gg\mu_m\mathcal{H}_0$, for the slope at $\bar{m}=1$ we find

$$\left(\frac{d\bar{m}}{d\bar{n}}\right)_{\bar{m}=1}\approx\frac{1}{\bar{n}_{0L}}e^{-w/2+x}. \tag{4.5}$$

Thus the *larger* of $\mu_m\mathcal{H}_0$ or $\Delta\epsilon/2$ determines the region of temperature stability for the step. In the case of Fig. 2, $\Delta\epsilon/2=0.9$ K and $\mu_m\mathcal{H}_0=16$ mK.

The points in the thermodynamic phase space that all isotherms seem to pass through will be called invariant points. In Fig. 2, there are three such points located at $(\bar{n},\bar{m})=(0,0),(\bar{n}_{\rm onset}/2,1),(\bar{n}_{\rm onset},4/3)$. (We note from Table I that $\bar{n}_{\rm onset}=\Delta\epsilon/\epsilon_{\rm F\diagup}=0.761$.) From Eqs. (3.8) and (3.10), we can write

$$1+(1+e^{-w})e^{-2x}\Lambda_{0+}+e^{-w}e^{-4x}\Lambda_{0+}^2=e^{w\diagup\bar{n}-x\bar{m}}. \tag{4.6}$$

In order to obtain the trivial invariant point at (0,0) we substitute $\bar{m}=0$ into Eqs. (4.2) and (4.6) to yield

$$1+(1+e^{-w})\Lambda_{0+}+e^{-w}\Lambda_{0+}^2=e^{w\diagup\bar{n}}. \tag{4.7}$$

We note that $\bar{n}=0$ is a self-consistent solution since in that limit $\Lambda_{0+}\sim e^{\beta\mu}\to 0$, at any temperature.

For the invariant point at $\bar{m}=1$, we use Eq. (4.3) in Eq. (4.6) to yield

$$2[\cosh(x)+\cosh(w/2)]=e^{w/\bar{n}}. \tag{4.8}$$

The low-temperature limit is controlled by the larger of x or $w/2$. For our system we find

$$\bar{n}\approx\frac{1}{2}\bar{n}_{\text{onset}}+O(e^{-w/2}). \tag{4.9}$$

Thus, in agreement with Fig. 2, for temperatures much less than $\Delta\epsilon/2$, all magnetization isotherms come exponentially close to this invariant point.

For the last invariant point at $\bar{n}=\bar{n}_{\text{onset}}$ and $\bar{m}=4/3$ there does not seem to be a simple expression relating the external field, level spacing, and density as Eq. (4.8). We note, however, that this point is special at zero temperature. From Table III, the magnetization as a function of density along the second ramp is given by $\bar{m}=1+(\bar{n}-\bar{n}_{0R})/3\bar{n}_{0L}$. Thus when evaluated at $\bar{n}_{\text{onset}}=\bar{n}_{0L}+\bar{n}_{0R}$ all field and level-spacing dependence cancels out, leaving the pure number 4/3. We shall use a low-temperature expansion to analyze this point. From Table III the ground-state chemical potential at $\bar{m}=4/3$ is given by $\mu=\epsilon_1^0-\mu_m\mathcal{H}_0/3$. Substituting this into the Λ's, [Eq. (3.3)] yields

$$\begin{aligned}\Lambda_{0+}&=e^{w+2x/3}, \quad \Lambda_{1+}=e^{2x/3},\\ \Lambda_{0-}&=e^{w-4x/3}, \quad \Lambda_{1-}=e^{-4x/3}.\end{aligned} \tag{4.10}$$

Then, from Eqs. (4.6) and (4.2), we find

$$\bar{m}=\frac{4}{3}+O(e^{-2x/3}), \tag{4.11}$$

$$\bar{n}=\bar{n}_{\text{onset}}+O(e^{-2x/3}). \tag{4.12}$$

These results show the invariant point character in the limit $x\gg1$. Figure 2 indicates, however, that this behavior is still present at higher temperatures.

Invariant points can also be seen in the space of chemical potential as a function of magnetization. Figure 3 shows chemical potential isotherms as a function of magnetization for $\mathcal{T}=10$, 50, 100, 150, 200, and 250 mK. There are evidently three invariant points in this region located at the values of the chemical potential given by $\mu=[\epsilon_0^0,\frac{1}{2}(\epsilon_0^0+\epsilon_1^0),\epsilon_1^0]$. The central point at $\bar{m}=1$ is the most interesting. From Eqs. (4.3), we have at this point $\Lambda_{0+}\Lambda_{0-}\Lambda_{1+}\Lambda_{1-}=1$. Thus from the definition of the $\Lambda's$ [Eq. (3.3)], we find the simple result

$$\mu=\frac{1}{2}(\epsilon_0^0+\epsilon_1^0). \tag{4.13}$$

Since this chemical potential value is independent of $\mathcal{T}$ and $\mathcal{H}_0$, *all* chemical potential isotherms must pass through $\bar{m}=1$ when $\mu=\frac{1}{2}(\epsilon_0^0+\epsilon_1^0)$. For the system of Fig. 2, the point $\{\mu=0.9,\bar{m}=1\}$ is the central invariant point in Fig. 3.

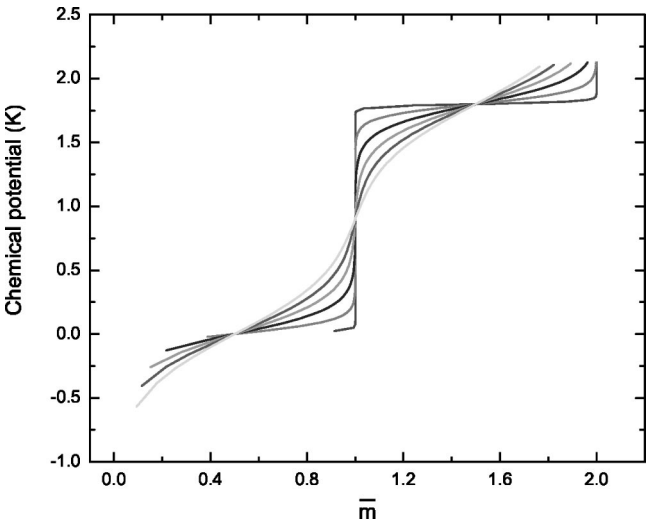

FIG. 3. Chemical potential μ as a function of magnetization $\bar{m}$, for temperatures = 10, 50, 100, 150, 200, and 250 mK.

The analysis of the two remaining points proceeds analogously. For the point at $\mu=\epsilon_0^0$, we have

$$\begin{aligned}\Lambda_{0+}&=e^{x}, \quad \Lambda_{1+}=e^{-w+x},\\ \Lambda_{0-}&=e^{-x}, \quad \Lambda_{1-}=e^{-w-x}.\end{aligned} \tag{4.14}$$

The magnetization is, therefore,

$$\bar{m}=\frac{1}{2x}\ln\left[e^{x}\frac{1+e^{-w+x}}{1+e^{-w-x}}\right]. \tag{4.15}$$

In the low-temperature limit $\beta\Delta\epsilon\gg1$ we find

$$\bar{m}\approx\frac{1}{2}+O(e^{-w}), \tag{4.16}$$

in agreement with Fig. 3. Similarly, for the point at $\mu=\epsilon_1^0$, we have

$$\begin{aligned}\Lambda_{0+}&=e^{w+x}, \quad \Lambda_{1+}=e^{x},\\ \Lambda_{0-}&=e^{w-x}, \quad \Lambda_{1-}=e^{-x}.\end{aligned} \tag{4.17}$$

The magnetization is therefore

$$\bar{m}=\frac{1}{2x}\ln\left[e^{x}\frac{1+e^{w+x}}{1+e^{w-x}}\right]. \tag{4.18}$$

In the low-temperature limit $\beta\Delta\epsilon\gg1$ we find

$$\bar{m}\approx\frac{3}{2}+O(e^{-w}), \tag{4.19}$$

in agreement with Fig. 3.

In Fig. 4, we show the pressure as a function of coverage at $\mathcal{T}=0$ and 10 mK and note that these are not distinguishable on the scale of the left hand axis in the figure. On the right hand axis, we have plotted the pressure difference $\delta\mathcal{P}=[\mathcal{P}(10\text{ mK})-\mathcal{P}(0)]$. At low coverages (in the first step) the pressures differ only by the constant factor

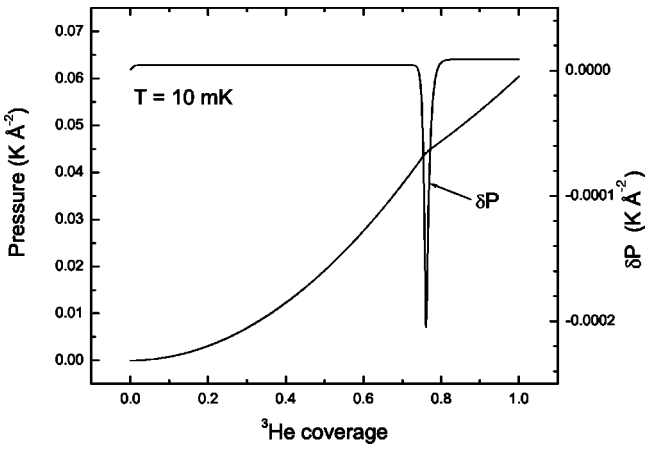

FIG. 4. Pressure as a function of coverage at T = 10 mK. We plot both $\mathcal{P}(\mathcal{T})$ from Eq. (3.15) and the zero-temperature pressure $\mathcal{P}(0)$ [Eq. (2.8)], along the left hand ordinate. The difference in the two pressures are not discernible on the scale of the left hand ordinate. The difference $\delta\mathcal{P}=\mathcal{P}(\mathcal{T})-\mathcal{P}(0)$ is plotted against the right hand ordinate. In the neighborhood of the density $\bar{n}_{\rm onset}\approx 0.761$, the pressure at finite temperature is lower than the pressure at zero temperature.

$\Sigma_{\alpha,s}\pi^2/(6\beta\lambda_T^2)=4.5\times10^{-6}$ K$-$Å^{-2}; see Eq. (3.22). In the coverage region near the end of the step where an additional Fermi sea will begin to be filled, we see from examining $\delta\mathcal{P}$ that the pressure at finite temperature drops *below* the zero temperature pressure. Thus we have the amazing result that for this system, an ideal Fermi gas, there is a regime in which the temperature derivative of the pressure is negative. This effect persists to surprisingly high temperatures as seen in the $\mathcal{T}=100$ mK data in Fig. 5.

One way to understand the source of this effect is to examine the shape of the zero-temperature and finite temperature isotherms. From Table II, we see that the pressure goes like $n^2/\nu_{\rm occ}$ in a region where $\nu_{\rm occ}$ number of Fermi seas are being filled. Thus the curvature of the equation of state parabola *decreases* as each new Fermi sea begins to be filled. The union of the parabolas then has kinklike features where two parabolas with differing curvatures are joined. The pressure at finite temperature, however, smoothly joins the two regions. The kinklike regions stick above the finite temperature curves and the result is that, in the coverage regime immediately surrounding the onset coverage of the filling of a new Fermi sea, the zero-temperature pressure is greater than the finite–temperature pressure. This behavior can be just barely seen in the equation of state of Fig. 5.

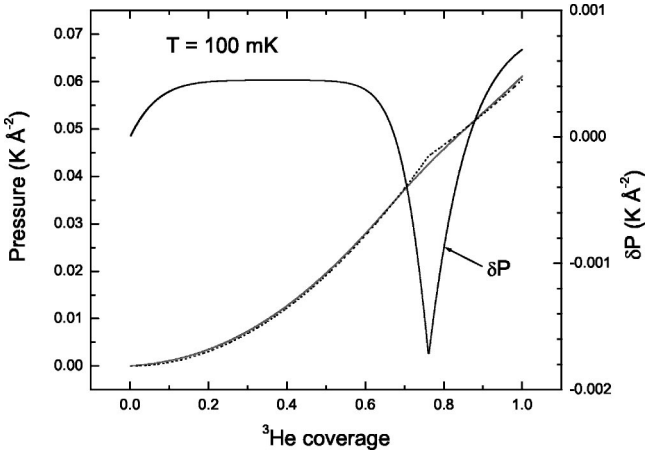

FIG. 5. Pressure as a function of coverage at T = 100 mK. We plot both $\mathcal{P}(\mathcal{T})$ from Eq. (3.15) and the zero-temperature pressure $\mathcal{P}(0)$ [Eq. (2.8)], along the left hand ordinate. The zero temperature pressure is plotted as a dashed line. The difference $\delta\mathcal{P}=\mathcal{P}(\mathcal{T})-\mathcal{P}(0)$ is plotted against the right hand ordinate. In the neighborhood of the density $\bar{n}_{\rm onset}\approx 0.761$, the pressure at finite temperature is lower than the pressure at zero temperature.

The physical and microscopic basis for this effect is the availability of a discrete set of states (i.e., the transverse single–particle states) that allow fermions to *spill over* from a filled Fermi sea into an unfilled Fermi sea under the action of a small temperature increase. It is straightforward to write down a model that contains the essence of this behavior.

For simplicity, we consider a $2d$ ^{3}He system at zero temperature with no magnetic field. The system is filled to the density $n=n_{\rm onset}$. That is, the ^{3}He atoms occupy the transverse ground-state up to the bottom of the band corresponding to the first excited state. We then increase the temperature slightly to $\delta\mathcal{T}$, keeping the number of particles fixed. A small number of particles $\delta\mathcal{N}$ will be promoted above the zero-temperature Fermi energy. These atoms will then distribute themselves equally over the occupied Fermi seas.

First, we will calculate an explicit expression for $\delta\mathcal{N}_{\alpha s}$, the number of particles in state $\{\alpha,s\}$ that are promoted above the zero-temperature Fermi-level at temperature $\delta\mathcal{T}$. From Eq. (3.1) we find

$$\delta\mathcal{N}_{\alpha s}=\frac{\mathcal{A}}{2\pi}\frac{m^*}{\hbar^2}\int_0^{\epsilon^0_{{\rm F}\alpha s}}d\epsilon\left(1-\frac{1}{e^{\beta(\epsilon-\epsilon^0_\alpha-\mu_m\mathcal{H}_0-\mu)}+1}\right), \tag{4.20}$$

where $\epsilon^0_{{\rm F}\alpha s}$ is the zero-temperature Fermi level, and $\beta=1/k_B\delta\mathcal{T}$. This expression can be integrated to yield

$$\delta\mathcal{N}_{\alpha s}=\frac{\mathcal{A}}{2\pi}\frac{m^*}{\hbar^2}\frac{1}{\beta}\ln\left(\frac{1+e^{x_F}}{1+e^{x_0}}\right), \tag{4.21}$$

where

$$x_F=\beta(\epsilon^0_{{\rm F}\alpha s}-\epsilon^0_\alpha-\mu_m\mathcal{H}_0-\mu), \tag{4.22}$$

$$x_0=\beta(-\epsilon^0_\alpha-\mu_m\mathcal{H}_0-\mu). \tag{4.23}$$

In the low-temperature limit, we can use Eq. (3.14) for the chemical potential to obtain $x_F=0$ and $x_0=-\beta\epsilon^0_{{\rm F}\alpha s}$, both to exponential order. Thus we find the simple result

$$(\delta\mathcal{N}_{\alpha s}/\mathcal{A})\lambda_T^2=\ln(2). \tag{4.24}$$

We set $\mathcal{H}_0=0$ and assume that we are at low enough temperature so that Eq. (3.22) accurately determines the pressure

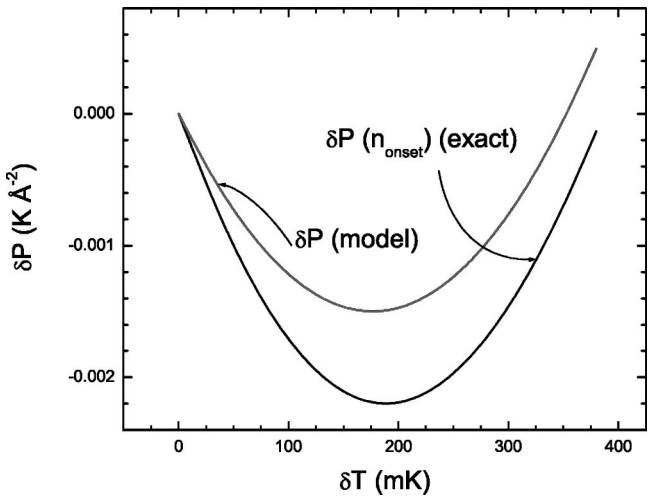

FIG. 6. Pressure change as a function of temperature at $n = n_{\text{onset}}$. We show the exact numerical results from Eqs. (2.8) and (3.20), and also the prediction of the simple model Eq. (4.27). The good qualitative agreement is in strong support of the explanation of the negative temperature derivative region as being due to ^{3}He atoms spilling over from a filled Fermi sea into an empty Fermi sea upon the application of a small increase in temperature.

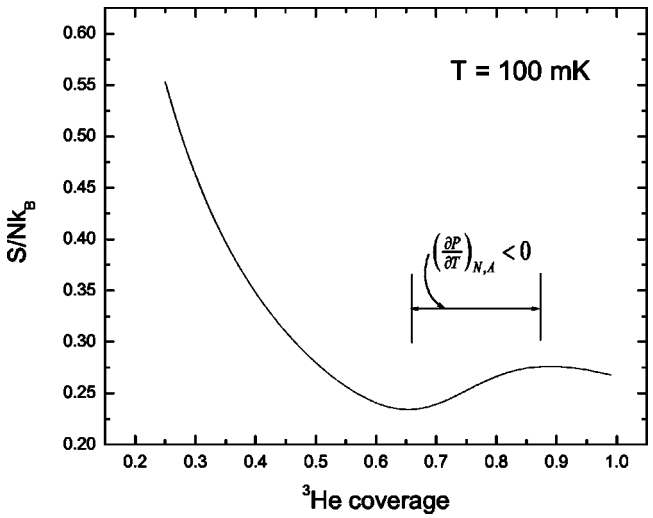

FIG. 7. The entropy per particle as a function of ^{3}He coverage at $\mathcal{T} = 100$ mK. The local maximum in the entropy between the coverages $\bar{n} = 0.654$ and 0.888 corresponds to the regime of negative temperature derivative for the pressure.

$$\mathcal{P} = \sum_{\alpha} \left[\frac{1}{2} \epsilon_{\mathrm{F}\alpha}(\mathcal{T}) n_{\alpha}(\mathcal{T}) + \frac{\pi^2}{3} \frac{1}{\beta \lambda_T^2} \right], \tag{4.25}$$

where in an obvious notation, $\epsilon_{\mathrm{F}\alpha}(\mathcal{T}) = (\hbar^2/2m^*) \times [2\pi n_{\alpha}(\mathcal{T})]$ and $n_{\alpha}(\mathcal{T}) = \Sigma_s n_{\alpha s}$. We now increase the temperature slightly to $\delta\mathcal{T}$. This drives $\delta\mathcal{N}$ of the particles above the zero-temperature Fermi level and from Eq. (4.24), $\delta\mathcal{N}/\mathcal{A} = 2\ln(2)/\lambda_T^2$. The pressure change $\delta\mathcal{P} = \mathcal{P}(\mathcal{T}) - \mathcal{P}(0)$ is given by

$$\delta\mathcal{P} = \frac{1}{2} \frac{\hbar^2}{2m^*} [2\pi (n_0(\mathcal{T})^2 - n_0^2 + n_1^2(\mathcal{T})] + \frac{\pi^2}{3} \frac{1}{\beta \lambda_T^2}. \tag{4.26}$$

In this simple model, we shall set the zero-temperature density at $n_0 = n_{\text{onset}}$, and choose the densities at finite temperature to be given by $n_0(\mathcal{T}) = n_{\text{onset}} - \frac{1}{2}(\delta\mathcal{N}/\mathcal{A})$ and $n_1(\mathcal{T}) = \frac{1}{2}(\delta\mathcal{N}/\mathcal{A})$. Thus we find

$$\delta\mathcal{P} = -\frac{1}{2} \ln(2) n_{\text{onset}} (k_{\mathrm{B}} \delta\mathcal{T}) + \left(\frac{\ln(2)^2}{4\pi} + \frac{\pi}{6} \right) \frac{m^*}{\hbar^2} (k_{\mathrm{B}} \delta\mathcal{T})^2. \tag{4.27}$$

The leading order term, corresponding to the decrease in pressure in the ground-state Fermi sea, is negative and dominates at very low temperature. In Fig. 6, we plot $\delta\mathcal{P}$ at $n = n_{\text{onset}}$ as a function of temperature, $\delta\mathcal{T}$. At every temperature, the exact $\delta\mathcal{P}$ is a minimum at this density (see, e.g., Figs. 4 and 5). The agreement between the parabola of the simple model and the exact calculation is qualitatively good, providing strong evidence that the picture of ^{3}He atoms spilling over the filled Fermi sea into the empty Fermi sea due to a small temperature increase is valid. We note that the temperature range over which $\delta\mathcal{P}$ is negative is, from Eq. (4.27), proportional to $\Delta\epsilon$, the level spacing. For the exact calculation, $\delta\mathcal{P}$ goes through zero at approximately 387 mK whereas, for the model, $\delta\mathcal{P}$ goes through zero at approximately 353 mK.

We can generalize this approach by assuming a variable fraction, x_0, of the particles promoted above the zero-temperature Fermi level are distributed between the two states. Thus, the densities at finite temperature are given by $n_0(\mathcal{T}) = n_{\text{onset}} - x_0(\delta\mathcal{N}/\mathcal{A})$ and $n_1(\mathcal{T}) = (1 - x_0)(\delta\mathcal{N}/\mathcal{A})$. For the calculation shown in Fig. 6 we set $x_0 = \frac{1}{2}$. We note, however, that the choice $x_0 = 0.605$ yields excellent agreement with the exact $\delta\mathcal{P}$.

There is an alternative way that this phenomenon can be examined. From a Maxwell relation

$$\left(\frac{\partial \mathcal{P}}{\partial \mathcal{T}} \right)_{\mathcal{N},\mathcal{A}} = \left(\frac{\partial S}{\partial \mathcal{A}} \right)_{\mathcal{N},\mathcal{T}} = -n^2 \left(\frac{\partial (S/\mathcal{N})}{\partial n} \right)_{\mathcal{N},\mathcal{T}}, \tag{4.28}$$

we see that the information that is present in the temperature derivative of the pressure also appears in the density derivative of the entropy per particle. In Fig. 7, we show the entropy per particle as a function of ^{3}He coverage at $\mathcal{T} = 100$ mK. The entropy per particle is not monotonic. The region of negative temperature derivative for the pressure creates a bumplike feature in the entropy versus coverage. The coverage interval over which the temperature derivative of the pressure is negative occurs between the local minimum and maximum as indicated on the figure. The possible importance of this observation is that the entropy can be obtained indirectly from experiment by integrating measured heat capacities, i.e., $C_{\mathcal{A}}/\mathcal{T}$.

Measurements of the mixture film heat capacities provided the first glimpse of the discrete transverse–state excitation spectrum for the ^{3}He component.[3,12] By definition, the heat capacity at a constant area is

$$C_{\mathcal{A}}=\left(\frac{\partial U}{\partial \mathcal{T}}\right)_{\mathcal{N},\mathcal{A}}. \tag{4.29}$$

It is convenient to study the dimensionless specific heat at constant area $C_{\mathcal{A}}/\mathcal{N}k_B$ since the high-temperature asymptotes are independent of coverage. The specific heat can be straightforwardly computed by numerically differentiating the internal energy from Eq. (2.9). Formally we can write

$$C_{\mathcal{A}}/\mathcal{N}k_B=\frac{1}{n}\sum_{\alpha,s}\left[\epsilon_\alpha^0-\mu_m\mathcal{H}_0 s\right]\left(\frac{\partial n_{\alpha s}}{\partial \mathcal{T}}\right)_{\mathcal{N},\mathcal{A}}+\frac{1}{n}\left(\frac{\partial \mathcal{P}}{\partial \mathcal{T}}\right)_{\mathcal{N},\mathcal{A}}. \tag{4.30}$$

One might hope that the explicit appearance of the $(\partial\mathcal{P}/\partial\mathcal{T})$ term in Eq. (4.30) might allow the specific heat to be a probe of the anomalous low-temperature behavior predicted for this quantity. Unfortunately, this is not the case as we shall now show. At low temperatures, $(\beta\epsilon_{\mathbf{k}}^{\alpha,s}\gg 1)$, we use Eq. (3.22) for the pressure. The low-temperature specific heat can then be written

$$C_{\mathcal{A}}/\mathcal{N}k_B=\frac{1}{n}\sum_{\alpha,s}\left[\epsilon_\alpha^0-\mu_m\mathcal{H}_0 s+\epsilon_{\mathrm{F}\alpha s}\right]\left(\frac{\partial n_{\alpha s}}{\partial \mathcal{T}}\right)_{\mathcal{N},\mathcal{A}}+\frac{\pi^2}{6}\frac{m^*}{\hbar^2\pi}k_B\mathcal{T}. \tag{4.31}$$

At low temperature, to exponential order, the term in square brackets is just the chemical potential [see Eq. (2.7)]; thus it can be taken out of the summation and the first term vanishes. This leaves the well-known limit

$$\lim_{\mathcal{T}\to 0}C_{\mathcal{A}}/\mathcal{N}k_B\sim\nu_{\mathrm{occ}}\frac{\pi^2}{6}\left(\frac{k_B\mathcal{T}}{\epsilon_{\mathrm{F}0}}\right), \tag{4.32}$$

where we remind the reader, that $\epsilon_{\mathrm{F}0}=(\hbar^2/2m^*)2\pi n$, and ν_{occ} is the number of occupied Fermi seas at zero temperature. This is of course equal to the low-temperature limit of the entropy, Eq. (3.25).

In Fig. 8, we show the calculated specific heats as a function of temperature and coverage. The specific heat at coverages less than $\bar{n}_{\mathrm{onset}}$ exhibit Schottky peaks. The peak structure becomes quite dramatic in the limit of low coverages. At the lowest coverage there is an interesting interplay between the Schottky peak at ≈ 0.7 K and the very large low−temperature slope from Eq. (4.32). The Schottky peak is a maximum at lowest coverage where the spacing between the chemical potential and the first excited state is a maximum. The peak diminishes in size with increasing coverage and disappears for $\bar{n}>\bar{n}_{\mathrm{onset}}$. This latter behavior is the result of the use of a two-state model. The availability of additional low-lying discrete levels could serve to wash out the Schottky peak. The actual system also has available a continuum set of states representing promotion out of the film into the vacuum. We note, however, that at low coverage, the first excited state seems to be located approximately 3 K below the vacuum level as illustrated in Figs. 45 and 46 of Ref. 1 and Table I of Ref. 4.

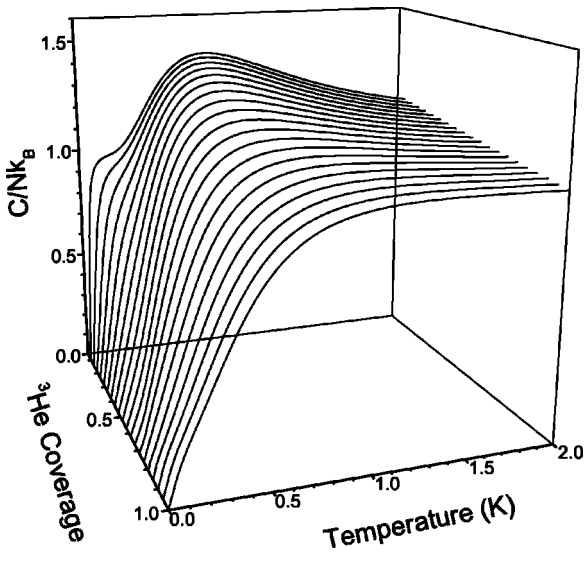

FIG. 8. Specific heat at constant area as a function of temperature and coverage shown in steps of $\Delta\bar{n}=0.05$. The disappearance of the Schottky peak for $\bar{n}>\bar{n}_{\mathrm{onset}}$ is due to the use of a two-state model.

As seen from Eq. (4.32), the low-temperature heat capacities have a dramatic dependence on the number of occupied states. This behavior was seen by Dann, Nyéki, Cowan, and Saunders,[13] and discussed by Anderson, Miller, and Hallock.[14] In Fig. 9, we show the specific heat as a function of ^{3}He coverage. The specific heat is normalized to $(\pi^2/6\epsilon_{\mathrm{F}0})\mathcal{T}$, the value of the specific heat for a single state being occupied. The ordinate is then effectively the number of occupied states. It is seen that in the region $\bar{n}<\bar{n}_{\mathrm{onset}}$ there are two occupied states (the first step) and in the region $\bar{n}>\bar{n}_{\mathrm{onset}}$ there are four occupied states (the second step).

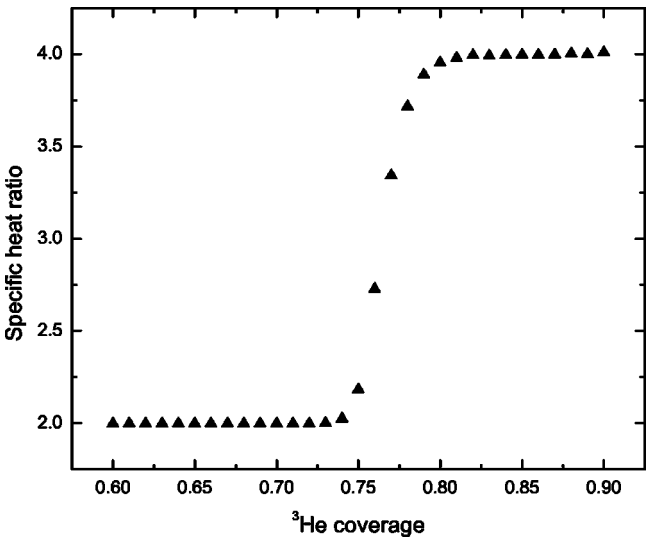

FIG. 9. The low-temperature ($\mathcal{T}\leqslant 10$ mK) specific heat as a function of ^{3}He coverage. The specific heat is normalized to $(\pi^2/6\epsilon_{\mathrm{F}0})k_B\mathcal{T}$. Thus the ordinate is a direct measure of the number of occupied Fermi seas.

Exact closed forms for both the heat capacity at constant area and the heat capacity at constant pressure can be obtained. We first consider the heat capacity at constant area. From Eq. (4.30) we have

$$C_{\mathcal{A}}=\sum_{\alpha,s}\left[\epsilon_{\alpha}^{0}-\mu_{m}\mathcal{H}_{0}s\right]\left(\frac{\partial\mathcal{N}_{\alpha s}}{\partial\mathcal{T}}\right)_{\mathcal{N},\mathcal{A}}+\frac{\beta_{\mathcal{P}}}{\kappa_{\mathcal{T}}}\mathcal{A}, \quad (4.33)$$

where

$$\left(\frac{\partial\mathcal{P}}{\partial\mathcal{T}}\right)_{\mathcal{N},\mathcal{A}}=\frac{\beta_{\mathcal{P}}}{\kappa_{\mathcal{T}}}. \quad (4.34)$$

$\beta_{\mathcal{P}}$ is the thermal expansion coefficient and $\kappa_{\mathcal{T}}$ is the isothermal compressibility. It is straightforward to derive expressions for both quantities:

$$\beta_{\mathcal{P}}=\frac{1}{\mathcal{A}}\left(\frac{\partial\mathcal{A}}{\partial\mathcal{T}}\right)_{\mathcal{N},\mathcal{P}}=n\kappa_{\mathcal{T}}\left(\frac{S}{\mathcal{N}}\right)-\frac{1}{\mathcal{T}}+\frac{1}{n\lambda_{T}^{2}\mathcal{T}}\sum_{\alpha,s}\left(\frac{\Lambda_{\alpha,s}}{1+\Lambda_{\alpha,s}}\right)y_{\alpha,s}, \quad (4.35)$$

and

$$\kappa_{\mathcal{T}}=-\frac{1}{\mathcal{A}}\left(\frac{\partial\mathcal{A}}{\partial\mathcal{P}}\right)_{\mathcal{N},\mathcal{T}}=\frac{1}{2\epsilon_{\mathrm{F}0}n}\sum_{\alpha,s}\left(\frac{\Lambda_{\alpha,s}}{1+\Lambda_{\alpha,s}}\right). \quad (4.36)$$

The temperature derivative of $\mathcal{N}_{\alpha s}$, at fixed $\mathcal{N}$ and $\mathcal{A}$, is given by

$$\left(\frac{\partial\mathcal{N}_{\alpha s}}{\partial\mathcal{T}}\right)_{\mathcal{N},\mathcal{A}}=\frac{\mathcal{N}_{\alpha s}}{\mathcal{T}}+\frac{\mathcal{A}}{\lambda_{T}^{2}}\left(\frac{\Lambda_{\alpha,s}}{1+\Lambda_{\alpha,s}}\right)\left[-\frac{y_{\alpha,s}}{\mathcal{T}}+\beta\left(\frac{\beta_{\mathcal{P}}}{n\kappa_{\mathcal{T}}}-\frac{S}{\mathcal{N}}\right)\right], \quad (4.37)$$

where we have used

$$\left(\frac{\partial\mu}{\partial\mathcal{T}}\right)_{\mathcal{N},\mathcal{A}}=\left(\frac{\beta_{\mathcal{P}}}{n\kappa_{\mathcal{T}}}-\frac{S}{\mathcal{N}}\right). \quad (4.38)$$

A simple check of Eq. (4.37) is to sum both sides over α and s. The left hand side vanishes and the right hand side reduces to Eq. (4.35). Thus the heat capacity at constant area can be written

$$C_{\mathcal{A}}=\frac{\mathcal{A}}{\lambda_{T}^{2}\mathcal{T}}\sum_{\alpha,s}\left(\epsilon_{\alpha}^{0}-\mu_{m}\mathcal{H}_{0}s\right)\left\{\left[n_{\alpha s}\lambda_{T}^{2}-\left(\frac{\Lambda_{\alpha,s}}{1+\Lambda_{\alpha,s}}\right)y_{\alpha,s}\right]+\left(\frac{\Lambda_{\alpha,s}}{1+\Lambda_{\alpha,s}}\right)\frac{1}{k_{\mathrm{B}}}\left(\frac{\beta_{\mathcal{P}}}{n\kappa_{\mathcal{T}}}-\frac{S}{\mathcal{N}}\right)\right\}+\mathcal{A}\frac{\beta_{\mathcal{P}}}{\kappa_{\mathcal{T}}}. \quad (4.39)$$

We need to check that $C_{\mathcal{A}}$ has the correct low-temperature limit [Eq. (4.32)]. The low-temperature limit of $y_{\alpha,s}$ at *fixed* $\mathcal{N}$ *and* $\mathcal{A}$ is given by

$$\lim_{\mathcal{T}\to 0}y_{\alpha,s}\sim\beta\epsilon_{\mathrm{F}\alpha s}=n_{\alpha s}\lambda_{T}^{2} \quad (4.40)$$

to exponential order. The low-temperature limit of $\beta_{\mathcal{P}}$ can most easily be obtained by rewriting Eq. (4.35) in terms of the enthalpy and using

$$\lim_{\mathcal{T}\to 0}\frac{\mathcal{H}}{\mathcal{N}}\sim\mu(\mathcal{T}=0)+\nu_{\mathrm{occ}}\frac{\pi^{2}}{6}\frac{(k_{\mathrm{B}}\mathcal{T})^{2}}{\epsilon_{\mathrm{F}0}}, \quad (4.41)$$

where we have used Eq. (3.22), and, from Eq. (2.7), the chemical potential at zero temperature is given by $\mu(\mathcal{T}=0)=\epsilon_{\alpha}^{0}-\mu_{m}\mathcal{H}_{0}s+\epsilon_{\mathrm{F}\alpha s}$. We find

$$\lim_{\mathcal{T}\to 0}\frac{\beta_{\mathcal{P}}}{n\kappa_{\mathcal{T}}}\sim\frac{S}{\mathcal{N}} \quad (4.42)$$

to exponential order. In this equation, the symbol $S/\mathcal{N}$ stands for the low-temperature limit of the entropy [Eq. (3.25)]. In Eq. (4.42), we have used the low-temperature limit of the isothermal compressibility:

$$\lim_{\mathcal{T}\to 0}\kappa_{\mathcal{T}}^{-1}\sim\frac{2n\epsilon_{\mathrm{F}0}}{\nu_{\mathrm{occ}}}. \quad (4.43)$$

This result is valid to exponential order for the limit taken at fixed $\mathcal{A}$ or fixed $\mathcal{P}$. Further, in the $\lim\mathcal{T}\to 0$, $\Lambda_{\alpha,s}\to\infty$ if the state $\{\alpha,s\}$ is occupied and is 0 otherwise. Thus, using Eqs. (4.40) and (4.42), the term in curly brackets in Eq. (4.39) vanishes in the low-temperature limit. Using Eqs. (4.42) and (3.25), the final term immediately reduces to the correct low-temperature limit [Eq. (4.32)].

An exact expression for the heat capacity at fixed pressure can also be obtained. By definition,

$$C_{\mathcal{P}}=\left(\frac{\partial H}{\partial\mathcal{T}}\right)_{\mathcal{N},\mathcal{P}}, \quad (4.44)$$

where $\mathcal{H}=U+\mathcal{P}\mathcal{A}$ is the enthalpy. Thus

$$C_{\mathcal{P}}=\sum_{\alpha,s}\left[\epsilon_{\alpha}^{0}-\mu_{m}\mathcal{H}_{0}s\right]\left(\frac{\partial\mathcal{N}_{\alpha s}}{\partial\mathcal{T}}\right)_{\mathcal{N},\mathcal{P}}+2\beta_{\mathcal{P}}\mathcal{P}\mathcal{A}, \quad (4.45)$$

where $\beta_{\mathcal{P}}$ is the thermal expansion coefficient [Eq. (4.35)]. The temperature derivative of $\mathcal{N}_{\alpha s}$ at fixed $\mathcal{N}$ and $\mathcal{P}$ is given by

$$\left(\frac{\partial\mathcal{N}_{\alpha s}}{\partial\mathcal{T}}\right)_{\mathcal{N},\mathcal{P}}=\frac{\mathcal{N}_{\alpha s}}{\mathcal{T}}+\frac{\mathcal{A}}{\lambda_{T}^{2}}\left(\frac{\Lambda_{\alpha,s}}{1+\Lambda_{\alpha,s}}\right)\left(-\frac{y_{\alpha,s}}{\mathcal{T}}-\beta\frac{S}{\mathcal{N}}\right)+\mathcal{N}_{\alpha s}\beta_{\mathcal{P}}. \quad (4.46)$$

A simple check of Eq. (4.46) is to sum both sides over α and s. The left hand side vanishes and the right hand side reduces to Eq. (4.35). Thus the heat capacity at constant pressure can be written

$$C_{\mathcal{P}}=\frac{\mathcal{A}}{\lambda_{T}^{2}\mathcal{T}}\sum_{\alpha,s}\left(\epsilon_{\alpha}^{0}-\mu_{m}\mathcal{H}_{0}s\right)\left[n_{\alpha s}\lambda_{T}^{2}(1+\beta_{\mathcal{P}}\mathcal{T})-\left(\frac{\Lambda_{\alpha,s}}{1+\Lambda_{\alpha,s}}\right)\left(y_{\alpha,s}+\frac{S}{\mathcal{N}k_{\mathrm{B}}}\right)\right]+2\mathcal{P}\mathcal{A}\beta_{\mathcal{P}}. \quad (4.47)$$

The low-temperature limit of $C_{\mathcal{P}}$ can be obtained by considering the quantity $C_{\mathcal{P}}-C_{\mathcal{A}}$. From Eqs. (4.45) and (4.33),

$$C_{\mathcal{P}}-C_{\mathcal{A}}=\sum_{\alpha,s}\left[\epsilon_\alpha^0-\mu_m\mathcal{H}_0 s\right]\left[\left(\frac{\partial\mathcal{N}_{\alpha s}}{\partial\mathcal{T}}\right)_{\mathcal{N},\mathcal{P}}-\left(\frac{\partial\mathcal{N}_{\alpha s}}{\partial\mathcal{T}}\right)_{\mathcal{N},\mathcal{A}}\right]+2\beta_{\mathcal{P}}\mathcal{P}\mathcal{A}-\beta_{\mathcal{P}}\mathcal{A}\kappa_{\mathcal{T}}^{-1},\tag{4.48}$$

Using Eqs. (4.37) and (4.46) we have

$$\left(\frac{\partial\mathcal{N}_{\alpha s}}{\partial\mathcal{T}}\right)_{\mathcal{N},\mathcal{P}}-\left(\frac{\partial\mathcal{N}_{\alpha s}}{\partial\mathcal{T}}\right)_{\mathcal{N},\mathcal{A}}=\beta_{\mathcal{P}}\mathcal{N}_{\alpha s}-\frac{\mathcal{A}}{n\lambda_T^2}\left(\frac{\Lambda_{\alpha,s}}{1+\Lambda_{\alpha,s}}\right)\beta\beta_{\mathcal{P}}\kappa_{\mathcal{T}}^{-1}.\tag{4.49}$$

We immediately find

$$C_{\mathcal{P}}-C_{\mathcal{A}}=\mathcal{A}\beta_{\mathcal{P}}{}^2\mathcal{T}\kappa_{\mathcal{T}}^{-1},\tag{4.50}$$

which is a well-known thermodynamic identity. In the low-temperature limit, we find

$$\lim_{\mathcal{T}\to 0}C_{\mathcal{P}}\sim C_{\mathcal{A}}\left[1+\nu_{\rm occ}{}^2\frac{\pi^2}{12}\left(\frac{k_{\rm B}\mathcal{T}}{\epsilon_{\rm F0}}\right)^2\right],\tag{4.51}$$

where in this expression, the symbol $C_{\mathcal{A}}$ is the low-temperature result given by Eq. (4.32) and we have used the low-temperature limit of $\beta_{\mathcal{P}}$, Eq. (4.42).

Another response function of interest in these systems is the magnetic susceptibility χ, at fixed system size. By definition,

$$\chi=\left(\frac{\partial\mathcal{M}}{\partial\mathcal{H}_0}\right)_{\mathcal{N},\mathcal{A},\mathcal{T}}.\tag{4.52}$$

This can be written as

$$\chi/\chi_0=\overline{m}+\mathcal{H}_0\left(\frac{\partial\overline{m}}{\partial\mathcal{H}_0}\right)_{\mu,\mathcal{A},\mathcal{T}}+\mathcal{H}_0\left(\frac{\partial\overline{m}}{\partial\mu}\right)_{\mathcal{N},\mathcal{A},\mathcal{H}_0}\left(\frac{\partial\mu}{\partial\mathcal{H}_0}\right)_{\mathcal{N},\mathcal{A},\mathcal{T}},\tag{4.53}$$

where χ_0 is the Pauli susceptibility defined as

$$\chi_0=\mathcal{M}_0/\mathcal{H}_0=\frac{m^*\mu_m^2\mathcal{A}}{\pi\hbar^2}.\tag{4.54}$$

We are interested in the susceptibility in the limit of zero applied field, $\mathcal{H}_0\to 0$. The first term in Eq. (4.53), the magnetization, vanishes in that limit because the system is paramagnetic. The third term has an explicit factor of $\mathcal{H}_0$ thus in order to show that it also vanishes in the zero-field limit, we only need show that the remaining two components do not blow up when $\mathcal{H}_0\to 0$. The second component is

$$\left(\frac{\partial\overline{m}}{\partial\mu}\right)_{\mathcal{N},\mathcal{A},\mathcal{H}_0}=\overline{m}\left(\frac{\beta_{\mathcal{P}}\mathcal{T}}{n\kappa_{\mathcal{T}}}-\frac{\mathcal{T}\mathcal{S}}{\mathcal{N}}\right)^{-1}+\frac{1}{2x}\sum_\alpha\left[\left(\frac{\Lambda_{\alpha+}}{1+\Lambda_{\alpha+}}\right)\times\left(\frac{\partial y_{\alpha+}}{\partial\mu}\right)-\left(\frac{\Lambda_{\alpha-}}{1+\Lambda_{\alpha-}}\right)\left(\frac{\partial y_{\alpha-}}{\partial\mu}\right)\right].\tag{4.55}$$

Using

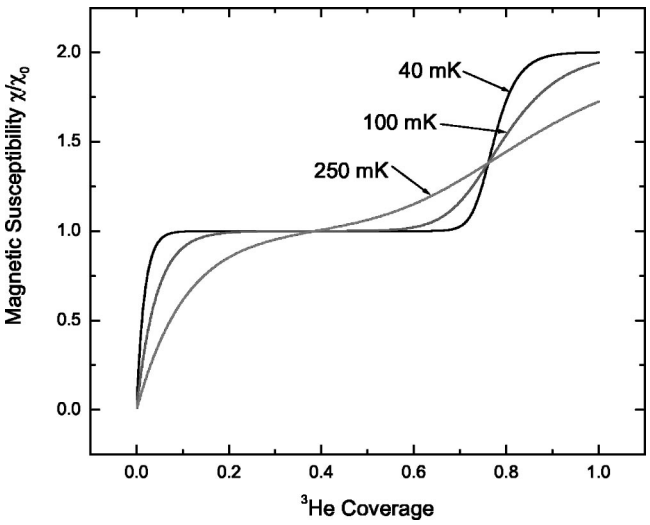

FIG. 10. Magnetic susceptibility in units of the Pauli susceptibility as a function of ^{3}He coverage at temperatures 40, 100, and 250 mK. At $\mathcal{T}=0$ K the susceptibility would be horizontal steps at $\chi/\chi_0=1$ and 2, with a vertical ramp at $\overline{n}_{0R}=0.77$.

$$\left(\frac{\partial y_{\alpha s}}{\partial\mu}\right)_{\mathcal{N},\mathcal{A},\mathcal{H}_0}=-y_{\alpha,s}\left(\frac{\beta_{\mathcal{P}}\mathcal{T}}{n\kappa_{\mathcal{T}}}-\frac{\mathcal{T}\mathcal{S}}{\mathcal{N}}\right)^{-1}+\beta,\tag{4.56}$$

it is clear that, in fact, Eq. (4.55) is well behaved in the limit of zero applied field. The final component of the third term can be evaluated using Eq. (3.13) and is also well behaved in the zero-field limit. Thus only the middle term survives, and we can write

$$(\chi/\chi_0)_{\mathcal{H}_0=0}=\sum_\alpha\frac{\Lambda_\alpha}{1+\Lambda_\alpha},\tag{4.57}$$

where $\Lambda_\alpha=\exp\beta(\mu-\epsilon_\alpha^0)$. In Fig. 10 we show the magnetic susceptibility at temperatures 40, 100, and 250 mK. This figure shows clearly that the magnetic susceptibility exhibits steps at integer values similar to the magnetization steps of Fig. 2. In the low-temperature limit, $\Lambda_\alpha\approx\exp\beta\mu\to\infty$; thus the sum in Eq. (4.57) yields a series of steps as each transverse state is occupied.

The magnetic susceptibility has two nontrivial invariant points. They are, in fact, located at the same values of the variables as the magnetization invariant points in Fig. 2. The first is at $\chi/\chi_0=1$. From Eq. (4.57), this implies $\mu=\frac{1}{2}(\epsilon_0^0+\epsilon_1^0)$, a result that is independent of temperature. The coverage at $\chi/\chi_0=1$ is given by

$$\overline{n}=\frac{1}{w_{\not\in}}\log(2+2\cosh w)\approx\frac{\Delta\epsilon}{2\epsilon_{\rm F\not\in}}+O(e^{-w/2}).\tag{4.58}$$

The second invariant point is at $\chi/\chi_0=4/3$. In the limit $e^{\beta\epsilon_1^0}\gg e^{\beta\epsilon_0^0}$, we find

$$\mu\approx\epsilon_1^0,\tag{4.59}$$

$$\overline{n}\approx\frac{\Delta\epsilon}{\epsilon_{\rm F\not\in}}+O(e^{-w}).\tag{4.60}$$

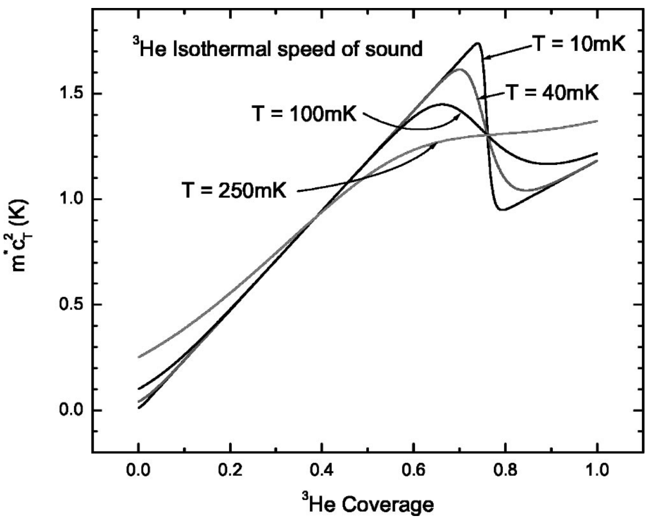

FIG. 11. Isothermal speed of sound $m^*c_{\mathcal{T}}^2$ as a function of ^{3}He coverage. The low-coverage degenerate region clearly shows a linear coverage dependence. The discontinuity in the speed of sound occurs each time a new Fermi sea begins to be occupied. There are two invariant points located at $\overline{n}=\overline{n}_{\rm onset}/2,\overline{n}_{\rm onset}$.

The final response function, the isothermal compressibility, $\kappa_{\mathcal{T}}$, is also sensitive to the filling of the Fermi seas. The compressibility was introduced in Eq. (4.36) during the discussion of the heat capacity. In the following we shall find it more useful to refer to the isothermal speed of sound. The compressibility and the speed of sound are related by $m^*c_{\mathcal{T}}^2=\kappa_{\mathcal{T}}^{-1}/n$. Thus from Eq. (4.36) we have

$$m^*c_{\mathcal{T}}^2=\frac{2\epsilon_{\rm F0}}{\sum_{\alpha,s}[\Lambda_{\alpha,s}/(1+\Lambda_{\alpha,s})]}. \qquad (4.61)$$

At zero temperature, the isothermal speed of sound is given by

$$(m^*c_{\mathcal{T}}^2)_{\mathcal{T}=0}=2\epsilon_{\rm F0}/\nu_{\rm occ}, \qquad (4.62)$$

where we remind the reader that $\epsilon_{\rm F0}$ is defined in Eq. (3.26) and $\nu_{\rm occ}$ is the number of occupied Fermi seas. Thus, at $\mathcal{T}=0$ K, the isothermal speed of sound has *discontinuous* decreases at each new ramp or step. In Fig. 11 we show $m^*c_{\mathcal{T}}^2$ as a function of ^{3}He coverage. The discontinuity appears at $\overline{n}_{0R}\approx\overline{n}_{1L}=0.76$; thus the drop in the speed of sound is given by $\Delta m^*c_{\mathcal{T}}^2=2(1.8\ {\rm K})(1/2-1/4)=0.9$ K. We note that the drop is calculated from the first step to the second step since, in this system, the intervening ramp occupies such a narrow density range. In terms of units of speed, $m^*c_{\mathcal{T}}^2=1$ K corresponds to $c_{\mathcal{T}}=45$ m/s.

There are two invariant points in this figure. They are basically invariant points of the density. Thus the high coverage invariant point is characterized by $\mu=\epsilon_1^0$, and we find

$$\overline{n}=\frac{\Delta\epsilon}{\epsilon_{{\rm F}\ell}}+O(e^{-w}). \qquad (4.63)$$

The low coverage invariant point occurs at $\mu=\frac{1}{2}\epsilon_1^0$ and we find

$$\overline{n}=\frac{1}{2}\frac{\Delta\epsilon}{\epsilon_{{\rm F}\ell}}+O(e^{-(1/2)\beta\epsilon_1^0}). \qquad (4.64)$$

We have assumed $w\gg x$ for both invariant points and for the latter we have also assumed that $\frac{1}{2}\epsilon_1^0>\epsilon_0^0$.

V. CONCLUSION

In this paper, we have examined the thermodynamic properties of an ideal Fermi gas model of ^{3}He in a thin ^{4}He superfluid film. We introduced a two-state model that is sufficient to describe the submonolayer coverage regime of interest. The physical parameters describing the system are shown in Table I and were determined by nuclear magnetic resonance experiments on a Nuclepore substrate.[2] The ^{3}He atoms have an effective mass of 1.38 m_3 and reside in a two-state external potential with a level spacing of $\Delta\epsilon=1.8$ K. The experimental magnetic energy is $\mu_m\mathcal{H}_0=15.6$ mK.

The magnetization as a function of coverage at zero temperature has a pair of steps whose position is determined by the relative sizes of the external field, $\mu_m\mathcal{H}_0$, and the level spacing $\Delta\epsilon$; see Table II. The ramps leading up to the steps signal regions where the Fermi sea of an unpaired spin state is being filled. On the steps all spin states are paired. In agreement with experiment,[2] Fig. 2 shows that the stepped magnetization structure survives through temperatures at least as high as 100 mK. In the text we show that the characteristic temperature over which the stepped structure survives is given by the larger of $\Delta\epsilon/2$ and $\mu_m\mathcal{H}_0$.

The chemical potential versus magnetization and the magnetization versus coverage both have invariant points where all isotherms pass exponentially close at low temperatures (as derived in the text). One of the chemical potential invariant points is valid at all temperatures and external fields. The magnetization versus coverage results are in good qualitative agreement with the experimental data of Higley, Sprague, and Hallock (see Fig. 3 of Ref. 2). The invariant points in the interacting system appear at the coverages given by Eqs. (4.9) and (4.12).

We calculated the spreading pressure as a function of coverage and temperature. The low-temperature results were obtained from Eq. (3.20), and an exact result valid for low temperature: $y_{\alpha,s}>0$. We found that there exist regions in the thermodynamic state space for which $d\mathcal{P}/d\mathcal{T}<0$. These regions are located near the corners of the magnetization steps where at zero temperature $d\mathcal{P}/dn$ is discontinuous. A simple model is introduced that qualitatively explains these anomalous regions as being due to ^{3}He atoms "spilling over" a filled Fermi sea into an available empty Fermi sea due to a small increase in temperature. We note that experiments on adsorbed films have been reported where spreading pressure is a variable that can be measured directly.[15,16] We noted that this behavior is also reflected in the coverage dependence of isotherms of the entropy per particle, a quantity

that can be indirectly determined from heat capacity measurements.

We investigated the behavior of the response functions: the heat capacity at fixed area and fixed pressure, the magnetic susceptibility, and the isothermal speed of sound. In Eqs. (4.39), (4.47), (4.57), and (4.61), respectively, we exhibit analytic expressions for each of these functions. In addition, in Eq. (4.35), we exhibit an exact expression for the thermal expansion coefficient, $\beta_{\mathcal{P}}$. These expressions, together with the entropy of Eq. (3.24), exhibit the explicit dependence of the response functions on the thermodynamic fields, $\mathcal{T}$, $\mathcal{P}$, μ, and $\mathcal{H}_0$.

In the limit of the two-state model, the specific heat at constant area exhibits a classical Schottky maximum at approximately 0.75 K that is very pronounced at low coverage. The peak diminishes with increasing coverage and disappears for $\overline{n} > \overline{n}_{\text{onset}}$ when the chemical potential crosses the bottom of the band of the first excited transverse state. As discussed above, if in the real system there are additional discrete states lying close to the first excited state then the Schottky peak will tend to get washed out. The slopes of the low-temperature specific heat (the specific heat effective masses) show a steplike change across the corners of the magnetization steps due to the different phase space available on either side. It is important to note that the specific heat that is being discussed is the heat capacity per particle and not the heat capacity per unit area. These two quantities have qualitatively different dependences on temperature. For the two-dimensional, ideal Fermi gas, the low-temperature slopes for the heat capacity per unit area are constants, whereas for the heat capacity per particle the low-temperature slopes go like 1/coverage. Similarly the high temperature asymptotes for the heat capacity per area are proportional to the coverage whereas for the heat capacity per particle the high-temperature asymptotes are a constant, unity.

In Fig. 10, we show the magnetic susceptibility versus ^{3}He coverage for this system. The susceptibility exhibits steps in the same qualitative fashion as the magnetization. The magnetic susceptibility was measured by Valles, Higley, Johnson and Hallock,[17] and was calculated for the fully interacting system by Krotscheck, Saarela, and Epstein.[18]

We show that the isothermal speed of sound exhibits discontinuities at zero temperature as a function of ^{3}He coverage. These discontinuities are still readily apparent at temperatures on the order of 100 mK, as shown in Fig. 11. We note that a prediction for the zero sound spectra for this system has been published elsewhere.[19] It is not clear to us whether density fluctuations of a normal Fermi liquid which floats in an inhomogeneous superfluid film will be isothermal as in a superfluid or adiabatic as in usual media. In any case, the adiabatic speed of sound, c_S can be related to the isothermal speed of sound, c_T, by means of the thermodynamic identity

$$c_S = \sqrt{\frac{C_P}{C_{\mathcal{A}}}}\, c_T, \tag{5.1}$$

where C_P and $C_{\mathcal{A}}$ are heat capacities at constant pressure and area, respectively. Thus, from Eq. (4.51), we immediately find the low-temperature relation

$$c_S \approx \left[1 + {\nu_{\text{occ}}}^2 \frac{\pi^2}{12}\left(\frac{k_B \mathcal{T}}{\epsilon_{F0}}\right)^2\right]^{1/2} c_T. \tag{5.2}$$

From Table I, we see that a full monolayer corresponds to a Fermi energy $\epsilon_{F0} = 2.37$ K. Thus, over much of the low–temperature phase diagram, there will be little difference in the sound speeds.

We note that by inspection of Eq. (4.36) for the isothermal compressibility and Eq. (4.57) for the zero–field, magnetic susceptibility, we find the relation

$$(\chi/\chi_0)_{\mathcal{H}_0 = 0} = (2\epsilon_{F0} n)\kappa_T. \tag{5.3}$$

Thus, *in the Fermi gas limit*, a measurement of the zero–field magnetic susceptibility is equivalent to a measurement of the isothermal speed of sound.

Higley, Sprague and Hallock[2] showed that good agreement with the magnetization experiment can be achieved by taking into account some effects of interactions. In work to be reported elsewhere, we have generalized Landau Fermi liquid theory in the spirit of Quader and Bedell[20] to the mixture films in order to include the effects of interactions.[21]

ACKNOWLEDGMENTS

The authors would like to express their appreciation to J. G. Dash for helpful input. Part of the work in this paper was done while one of the authors (M.D.M.) was on leave at the Institut für Theoretische Physik, Johannes-Kepler-Universität, Linz, Austria and he is grateful for their support.

*Electronic address: mdm@wsu.edu

[1] R. B. Hallock, in *Progress in Low Temperature Physics* (Elsevier/North-Holland, Amsterdam, 1995), Vol. XIV, p. 321.
[2] R. H. Higley, D. T. Sprague, and R. B. Hallock, Phys. Rev. Lett. **63**, 2570 (1989).
[3] M. J. DiPirro and F. M. Gasparini, Phys. Rev. Lett. **44**, 269 (1980).
[4] F. M. Gasparini, B. Bhattacharyya, and M. J. DiPirro, Phys. Rev. B **29**, 4921 (1984).
[5] B. K. Bhattacharyya, M. J. DiPirro, and F. M. Gasparini, Phys. Rev. B **30**, 5029 (1984).
[6] D. S. Sherrill and D. O. Edwards, Phys. Rev. B **31**, 1338 (1985).
[7] R. A. Guyer, Phys. Rev. Lett. **53**, 795 (1984).
[8] R. H. Anderson and M. D. Miller, Phys. Rev. B **40**, 2109 (1989).
[9] R. H. Anderson and M. D. Miller, Phys. Rev. B **48**, 10 426 (1993).
[10] R. H. Anderson, J. Low Temp. Phys. **60**, 1 (1985).
[11] L. D. Landau and E. M. Lifshitz, *Quantum Mechanics* (Pergamon, New York, 1977).
[12] B. K. Bhattacharyya and F. M. Gasparini, Phys. Rev. B **31**, 2719 (1985).
[13] M. Dann, J. Nyéki, B. Cowan, and J. Saunders, J. Low Temp. Phys. **110**, 627 (1998).

[14] R. H. Anderson, M. D. Miller, and R. B. Hallock, Phys. Rev. B **59**, 3345 (1999).
[15] J. G. Dash, J. Suzanne, H. Schechter, and R. E. Peierls, Surf. Sci. **60**, 411 (1976).
[16] J. G. Dash, J. Suzanne, H. Shechter, and R. E. Peierls, Surf. Sci. **72**, 219 (1978).
[17] J. M. Valles, R. H. Higley, B. R. Johnson, and R. B. Hallock, Phys. Rev. Lett. **60**, 428 (1988).
[18] E. Krotscheck, M. Saarela, and J. L. Epstein, Phys. Rev. Lett. **61**, 1728 (1988).
[19] R. H. Anderson and M. D. Miller, Phys. Rev. B **66**, 014526 (2002).
[20] K. F. Quader and K. S. Bedell, J. Low Temp. Phys. **58**, 89 (1985).
[21] R. H. Anderson, E. Krotscheck, and M. D. Miller (unpublished).